On the Numerical Dispersion of the Radial Point Interpolation Meshless Method

Shunchuan Yang, Zhizhang Chen, *Fellow, IEEE*, Yiqiang Yu, and Sergey Ponomarenko

***Abstract*—The numerical dispersion of the time-domain radial point interpolation meshless (RPIM) method is investigated in this letter. It is found that numerical dispersion relationship of RPIM method shares the same form as that of a second-order central finite-difference time-domain method but with the additional factor introduced by the radial basis functions, when i) the two methods deploy the same nodal distribution for problem-domain discretization and ii) the local support domain of the RPIM method is defined to enclose only four adjacent nodes. Such an observation indicates that the RPIM method is a more general method and can be reduced to the conventional finite-difference time-domain method under certain conditions. In addition, comparisons between the meshless method and the finite-difference time-domain method are shown under different conditions.**

***Index Terms*—Finite-difference time-domain (FDTD), meshless, numerical dispersion, radial point interpolation meshless (RPIM).**

I. Introduction

UNLIKE the conventional grid-based methods such as the finite-difference time-domain (FDTD) method [1], the finite element method (FEM) [2] and the moment of method (MOM) [3], meshless methods interpolate fields to be solved with the field values at predefined scattering nodes in a support domain. A set of algebraic equations based on positions of the scattering nodes in a solution domain is then established and solved by linear solvers. That means that unlike grid-based methods, connection information among nodes is not required, which leads to easy implementation and high flexibility in modeling complex structures. As a result, the number of the published reports on the meshless methods for solving electromagnetic problems has increased dramatically. In particular, the smoothed particle electromagnetic method [4] and the radial point interpolation meshless (RPIM) method [5] have been proposed. Other forms of the meshless methods including the leapfrog and alternatively-direction-implicit RPIM methods in the time-domain are summarized in [6]. However, to the best of the authors' knowledge, no numerical dispersion of the meshless methods has been reported so far. In addition, no direct relationship between the FDTD method and RPIM method have been shown although it is mentioned in [7] that the RPIM method may reduce to the FDTD method under certain conditions (but no theoretical proof was given there).

In this letter, we fill in the void by investigating the numerical dispersion of the RPIM method and the relationship between the RPIM method and the FDTD method in terms of the numerical dispersion relationship. In addition, we will discuss the relationship between the shape parameter and the numerical dispersion of RPIM method. Due to limited space, we restrict our studies to the leapfrog time-domain meshless method.

II. Dispersion Analysis

To obtain analytical expressions of the numerical dispersion of the RPIM method, the spectral Fourier transform is applied, similar to that for the FDTD method presented in [8], [9]. For arbitrary numbers and positioning of nodes, numerical dispersion formulations of the RPIM method may not be practically meaningful due to their varieties used by different users, in addition to the difficulty in finding the associated formulations. Therefore, in this letter, we consider the case where the nodes are positioned in the same grid placement as that in the Yee's grid for the conventional FDTD method. In other words, in a support domain of a node, we consider one field component at one node, four H-nodes associated with one E-node and four E-nodes associated with one H-node, in a three dimensional setting. For the time domain discretization, we use the second-order central finite-difference scheme for the RPIM method. That means we can obtain the so-called leap-frog scheme for the time-marching equations [10].

By applying the spatial Fourier transformation to the meshless time-domain formulations [10], we can obtain the time-marching equations in the spectral domain. For example, take E_z component for the illustration purpose. The time-marching equation for E_z is then

$$E_{z,i}^{n+1/2} = E_{z,i}^{n+1/2} + \frac{\Delta t}{\varepsilon}\left(\sum H_{y,j}^{n+1/2}\partial_x \Phi_j - \sum H_{x,j}^{n+1/2}\partial_y \Phi_j\right) \quad (1)$$

where Φ_j is the shape function corresponding to node j in the local support domain. We can express the shape function in the vector form for all nodes as $\mathbf{\Phi} = [\,\Phi_1 \quad \Phi_2 \quad \cdots \quad \Phi_N\,]$, where $\mathbf{\Phi} = \mathbf{B}\mathbf{G}^{-1}$ with the RBF vector $\mathbf{B}$ and interpolation matrix $\mathbf{G}$. $\mathbf{G}$ can be expressed as

$$\mathbf{G} = \begin{bmatrix} 1 & e^{-\alpha(r/r_{\max})^2} \\ e^{-\alpha(r/r_{\max})^2} & 1 \end{bmatrix} \quad (2)$$

Manuscript received January 09, 2014; revised May 05, 2014; accepted June 20, 2014. Date of publication July 22, 2014; date of current version October 02, 2014.

S. Yang, Z. Chen, and Y. Yu are with the School of Electronic Engineering, The University of Electronic Science and Technology, Chengdu 610051, China and also with the Department of Electrical and Computer Engineering, Dalhousie University, Halifax, NS, B3J 2X4 Canada.

S. Ponomarenko is with the Department of Electrical and Computer Engineering, Dalhousie University, Halifax, NS, B3J 2X4 Canada.

Digital Object Identifier 10.1109/LMWC.2014.2340696

$r_{\max}$ is the maximum radius of the local support domain, which is taken in such a way that only four nodes are located in the support domain [10]; r is the distance between the two nodes in the local support domain. Thus, the first order partial derivative of the RBF vector $\mathbf{B}$ can be stated as

$$\partial_\xi \mathbf{B} = e^{-\alpha(r/2r_{\max})^2} \frac{\alpha \Delta\xi}{{r_{\max}}^2} [-1 \quad 1] \tag{3}$$

where $\xi = x, y$ and z and α is named as the shape parameter which can be found in [10]. Thus, the partial derivative of the shape function with respect to ξ can be obtained as

$$\partial_\xi \mathbf{\Phi} = \partial_\xi \mathbf{B}\mathbf{G}^{-1} = \frac{\Delta\xi\alpha}{{r_{\max}}^2} \frac{e^{-\alpha(r/2r_{\max})^2}}{-1 + e^{-\alpha(r/r_{\max})^2}} [1 \quad -1]. \tag{4}$$

By substituting (4) into (1) the following equation is obtained in the spectral domain:

$$E_z^{n+1/2} = E_z^{n-1/2} + j\frac{2\Delta t}{\Delta y \varepsilon} \sin\left(\frac{k_y \Delta y}{2}\right) \Delta y M_y H_x^n - j\frac{2\Delta t}{\Delta x \varepsilon} \sin\left(\frac{k_x \Delta x}{2}\right) \Delta y M_x H_y^n. \tag{5}$$

Here $M_\xi = (\Delta\xi\alpha/{r_{\max}}^2)(e^{-\alpha(r/2r_{\max})^2}/(-1 + e^{-\alpha(r/r_{\max})^2}))$ and k_ξ is the spatial frequency in the ξ direction.

Other field components can also be obtained in a similar manner.

With the similar process as described in [8], [9], the final dispersion relationship can be obtained as

$$\left(\sin\left(\frac{w\Delta t}{2}\right)\right)^2 = \frac{\Delta t^2}{\mu\varepsilon}\left[\left(\frac{M_{xx}\sin\left(\frac{k_x\Delta x}{2}\right)}{\Delta x}\right)^2 + \left(\frac{M_{yy}\sin\left(\frac{k_y\Delta y}{2}\right)}{\Delta y}\right)^2 + \left(\frac{M_{zz}\sin\left(\frac{k_z\Delta z}{2}\right)}{\Delta z}\right)^2\right] \tag{6}$$

with $M_{\xi\xi} = \Delta\xi M_\xi$. Equation (6) looks like the numerical dispersion relation of the conventional FDTD method with the addition of factors $M_{\xi\xi}$ on the right hand side.

Noticeably, we can see that when $\Delta\xi$ and α approaches zeros, respectively

$$\lim_{\Delta\xi\to 0} M_{\xi\xi} = \lim_{\Delta\xi\to 0} \frac{\Delta\xi^2\alpha}{{r_{\max}}^2} \frac{e^{-\alpha(r/2r_{\max})^2}}{-1 + e^{-\alpha(r/r_{\max})^2}} = -1 \tag{7}$$

and

$$\lim_{\alpha\to 0} M_{\xi\xi} = \lim_{\alpha\to 0} \frac{\Delta\xi^2\alpha}{{r_{\max}}^2} \frac{e^{-\alpha(r/2r_{\max})^2}}{-1 + e^{-\alpha(r/r_{\max})^2}} = -1. \tag{8}$$

The above results mean that the final numerical dispersion (6) becomes the analytic dispersion, $\omega^2\mu\varepsilon = k_x^2 + k_y^2 + k_z^2$, when shape parameter α, time step Δt and spatial step or distance between nodes $\Delta\xi$ approach to zero. When shape parameter α goes to zero, (6) becomes identical to the dispersion of FDTD [1]. As a result, the FDTD method can be considered as a special case of RPIM method. This can also be easily seen from (1): when α goes to zero, (4) becomes $-1/\Delta\xi$ and by substituting it into (1), we can obtain the updating formulation for the FDTD.

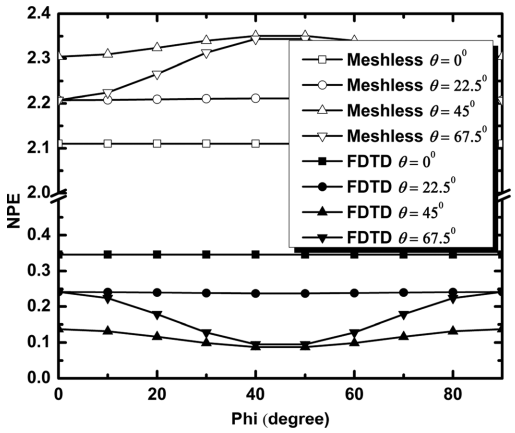

Fig. 1. *NPE* of the meshless method with $\alpha = 0.1$ and the FDTD method; $\mathrm{PPW} = 20$ and $\mathrm{CFLN} = 1$.

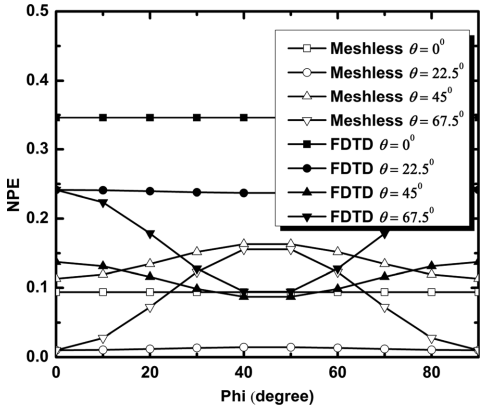

Fig. 2. *NPE* of the meshless method with $\alpha = 0.01$ and the FDTD method; $\mathrm{PPW} = 20$ and $\mathrm{CFLN} = 1$.

III. Numerical Results and Discussion

The shape parameter α plays an important role in RPIM method. In [11], the relationship between stability of the time-iteration of RPIM method and the shape parameter is presented. In this section, we discuss how the shape parameter affects the numerical dispersion.

To measure the numerical dispersion error, the numerical phase error (NPE) per unit length is defined and used [8]

$$NPE = \left|\frac{k_{num} - k_0}{k_0}\right| = \left|\frac{c - c_{num}}{c_{num}}\right| \tag{9}$$

where k_0 is the theoretical wave number, k_{num} is numerical wave number, $c = \omega/k_o$ is the speed of light in the continuous medium and $c_{num} = \omega/k_{num}$ is the speed of numerical waves with the RPIM method. ω is the angular frequency.

In the calculations

$$\begin{aligned} k_x &= k_{num}\sin\theta\cos\varphi \\ k_y &= k_{num}\sin\theta\sin\varphi \\ k_z &= k_{num}\cos\theta. \end{aligned} \tag{10}$$

Here θ and φ are the propagation angles in the horizontal and vertical planes, respectively.

Figs. 1 – 4 show *NPE* of the meshless method with different values of shape parameter α and that of the FDTD method. The spatial step is 1/20 of the wavelength, i.e., the spatial sampling

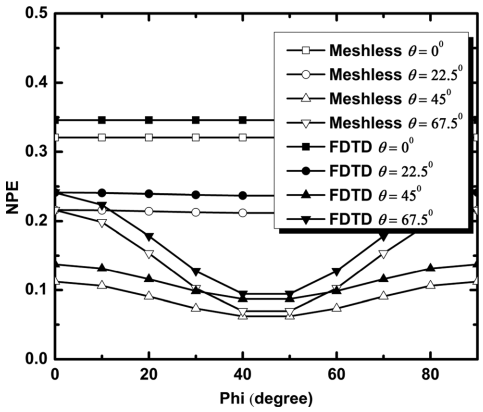

Fig. 3. NPE of the meshless method with $\alpha = 0.001$ and the FDTD method with $\mathrm{PPW} = 20$ and $\mathrm{CFLN} = 1$.

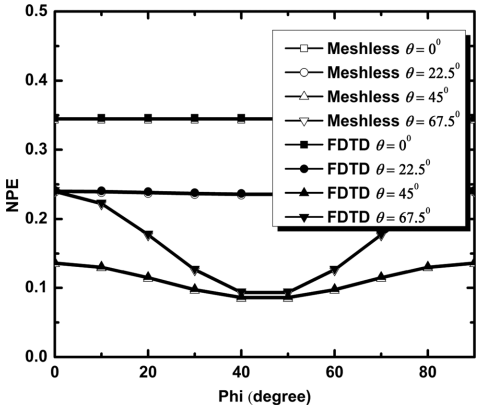

Fig. 4. NPE of the meshless method with $\alpha = 0.0001$ and the FDTD method with $\mathrm{PPW} = 20$ and $\mathrm{CFLN} = 1$.

is 20 points per wavelength (PPW). $r_{\max}$ equals to the spatial step. The time step was selected to be the same for both methods in order to make a fair comparison: it is the maximum time limit of the FDTD method, or the CFL number is one ($\mathrm{CFLN} = 1$).

It is easily seen from the figures that when $\alpha = 0.1$, *NPE* of the meshless method reaches its maximum at $\theta = 45°$ and its minimum at $\theta = 0°$. However, for the FDTD method, the numerical dispersion arrives at its minimum when $\theta = 45°$ and maximum when $\theta = 0°$. Therefore, numerical dispersions of the two methods show totally different properties but this difference becomes smaller when shape controlling parameter α becomes smaller.

When $\alpha = 0.1$, the maximum numerical dispersion errors of the meshless method is about as seven times of that of the FDTD method. However, when $\alpha = 0.01$, the situation reverses: the maximum numerical dispersion errors are smaller than that of the FDTD method. When $\alpha = 0.001$, the numerical dispersion errors of the two methods becomes similar. When $\alpha = 0.0001$, they become indistinguishable. That confirms our previous analysis result that when α approaches to zero, the numerical dispersion of the meshless method and the FDTD method becomes exactly the same. This indicates that the shape parameter α plays an important role on the numerical dispersion and the convergence of the meshless method to the FDTD method with better accuracy. Therefore, a reasonable value should be selected in the practical simulations. It should be also noted that although better convergence is achieved with small sharp parameter, it also comes with a smaller number of stable time iterations [11]. The balance should be taken between the stability condition and the accuracy. In our case study, we chose $\alpha = 0.018$ where the maximum numerical dispersion errors of RPM method equals to that of FDTD method. However, the optimized shape parameters are on a case-by-case basis; in [12], the authors proposed an automatic approach to search for the reasonable value with respect to a specific case.

IV. Conclusion

In this letter, numerical dispersion of the RPIM method is shown and its comparisons with that of the FDTD method are presented. Analytical derivations show that the numerical dispersion of the RPIM method is exactly the same as that of the FDTD method when the shape parameter α approaches zero. It indicates that the meshless method is a general method which can include the conventional FDTD method as its special case. Different numerical dispersion results based on various shape parameters are illustrated. The analysis shows that shape parameter should be selected carefully in the practical simulations to obtain small numerical dispersion errors and good stability.

References

[1] A. Taflove and S. C. Hagness, *Computationai Electrodynamics: The Finite-Difference Time-Domain Method*. Norwood, MA: Artech House, 1996.

[2] J. Jin, *The Finite Element Method in Electromagnetics*. New York: Wiley, 2002.

[3] R. F. Harrington and J. L. Harrington, *Field Computation by Moment Methods*. New York: Oxford Univ. Press, 1996.

[4] G. Ala, E. Francomano, A. Tortorici, E. Toscano, and F. Viola, "Smoothed particle electromagnetics: A mesh-free solver for transients," *J. Comput. Appl. Math.*, vol. 191, pp. 194–205, Jul. 2006.

[5] S. Lai, B. Wang, and Y. Duan, "Meshless radial basis function method for transient electromagnetic computations," *IEEE Trans. Magn.*, vol. 44, pp. 2288–2295, Oct. 2008.

[6] T. Kaufmann *et al.*, "Recent developments of the meshless radial point interpolation method for time-domain electromagnetics," *Int. J. Numer. Modelling: Electronic Networks, Devices Fields*, vol. 25, no. 5–6, pp. 468–489, Dec. 2012.

[7] T. Kaufmann, C. Fumeaux, and R. Vahldieck, "The meshless radial point interpolation method for time-domain electromagnetics," in *IEEE MTT-S Int. Dig.*, Atlanta, GA, Jun. 15–20, 2008, pp. 61–64.

[8] S.-C. Yang, Z. Chen, Y. Yu, and W.-Y. Yin, "An unconditionally stable one-step arbitrary-order leapfrog ADI-FDTD method and its numerical properties," *IEEE Trans. Antennas Propag.*, vol. 60, pp. 1995–2003, Apr. 2012.

[9] Z. Chen and S. Luo, "Generalization of the finite-difference-based time-domain methods using the method of moments," *IEEE Trans. Antennas Propag.*, vol. 54, pp. 2515–2524, Sep. 2006.

[10] Y. Yu and Z. Chen, "A 3-D radial point interpolation method for meshless time-domain modeling," *IEEE Trans. Microw. Theory Techn*, vol. 57, pp. 2015–2020, Aug. 2009.

[11] T. Kaufmann, C. Engstrom, C. Fumeaux, and R. Vahldieck, "Eigenvalue analysis and longtime stability of resonant structures for the meshless radial point interpolation method in time domain," *IEEE Trans. Microw. Theory Tech.*, vol. 58, pp. 3399–3408, Dec. 2010.

[12] P. Machado *et al.*, "An automatic methodology for obtaining optimum shape factors for the radial point interpolation method," *J. Microw., Optoelectron. Electromag. Appl.*, vol. 10, no. 2, pp. 389–401, Dec. 2011.